Mechanical properties of clusters in quasicrystal approximants: The example of the 1/1 Al-Cu-Fe approximant

Daniel Y. Jung and Walter Steurer*

Laboratory of Crystallography, Department of Materials, ETH Zurich, Wolfgang-Pauli-Strasse 10, 8093 Zurich, Switzerland

(Received 28 April 2011; published 15 August 2011)

Quantum-mechanical molecular dynamics have been used to investigate structural and physical properties of the 1/1 approximant of the icosahedral Al-Cu-Fe quasicrystal. Particular local structural arrangements of atoms, referred to here as clusters, have been analyzed with respect to their properties within the crystal structure. Artificial strain and cracks have been introduced to probe their mechanical properties, and artificial surfaces have been created to investigate their role for surface termination. From the energetics of the *ab initio* calculations results that flat surfaces cutting clusters are favored over puckered surfaces keeping clusters intact. The Vienna Ab-initio Simulation Package (VASP) was used for all calculations.

DOI: 10.1103/PhysRevB.84.054116 PACS number(s): 61.44.Br, 61.50.Ah, 61.50.Lt, 71.15.Nc

I. INTRODUCTION

The cluster-based description of complex crystal structures can be a powerful tool not only for their visualization and easy identification, but also for understanding the underlying geometrical building principles. In the case of complex intermetallics, such as quasicrystals and their approximants, one must be aware that the term "cluster" is used to describe recurrent structural units. It does not necessarily imply, but also not exclude, that they differ in chemical bonding or stoichiometry from their atomic environment or that they are mechanically stable units.[1,2] A recent good example for the usefulness of the cluster description are some intermetallics in the system Al-Cu-Ta with structures containing up to more than 23,000 atoms per giant unit cell.[3]

In the case of quasicrystals, employing covering clusters[4,5] allows more realistic growth models than using unit tiles supplied with matching rules. Furthermore, it is well known that orbital hybridization of atoms in the cluster core can lead to a pseudogap at the Fermi energy contributing to the stabilization of quasicrystals.[6,7] Therefore, at least the innermost part of the fundamental building clusters of quasicrystals can have some physical relevance.

The kind of interactions within and between the fundamental building clusters are still the subject of discussion. Studies of their mechanical properties by cleavage of quasicrystals and subsequent analysis of their surfaces[8–10] as well as by molecular dynamics simulations[11] did not lead to clear results. There is still an ongoing discussion pro and contra the mechanical stability of the clusters.[12–14] This was the motivation for our first-principle calculations performed for a better understanding of the inter- and intracluster interactions with focus on the mechanical properties. This work focuses mainly on static equilibrium surfaces; no kinetic or non-equilibrium processes have been included. The stabilizing effects of complete cluster shells terminating the surfaces as compared to flat surfaces have been investigated.

II. METHODOLOGY

All calculations have been performed with the VASP[15] code. The generalized gradient approximation[16] together with the projector augmented wave[17,18] method have been applied to calculate energies of the different structures at zero kelvin. In all calculations, the following projector augmented wave potentials were used: core region cutoffs are 1.9 atomic units (a.u.) for aluminum (core configuration $1s^2 2s^2 p^6$), 2.0 a.u. for copper (core configuration $1s^2 2s^2 p^6 3s^2$), 2.2 a.u. for iron (core configuration $1s^2$), and 2.0 a.u. The default plane wave cutoff energy for all calculations proved to be reliable and computationally acceptable. For the Brillouin zone sampling, the Monkhorst-Pack scheme[19] was employed with a $6 \times 6 \times 6$ k-point mesh for the single unit cell and $2 \times 4 \times 4$ mesh for the $2 \times 1 \times 1$ supercells. Convergence of energy and stress with respect to the mesh density was tested for each structure individually. The atoms were relaxed with the conjugate gradient and the steepest descent methods. The energy minimization procedure is iterative and proceeds until self-consistency within a prescribed tolerance of 10^{-5} eV per unit cell for electronic optimization and 10^{-4} eV per unit cell for atomic relaxation.

The electron localization function (ELF)[20,21] is a measure of the likelihood of finding an electron in the neighborhood space of a reference electron located at a given point and with the same spin. Physically, this measures the extent of spatial localization of the reference electron and provides a method for the mapping of electron pair probability in multielectronic systems. The ELF represents the organization of chemical bonding in direct space. Furthermore, it is a dimensionless localization index that expresses electron localization with respect to the uniform electron gas, whereas ELF $= 1$ corresponds to perfect localization and ELF $= 1/2$ to the electron gas. In ideal metals, there would not be any ELF maxima between the atoms but only around their centers, reflecting the shell structure of the core electrons. The ELF was calculated with the according module provided with the VASP code. For an overview, see the ELF website (http://www.cpfs.mpg.de/ELF).

Bader analysis[22,23] is an intuitive way of dividing molecules or crystal structures into atoms. Thereby, the definition of an atom is based purely on the electronic charge density and zero-flux surfaces are being used for separating atoms. A zero-flux surface is a two-dimensional surface across which the charge density has a minimum. Bader analysis can be used to calculate the volume that single atoms occupy in a

structure; additionally, the charge within this volume can be integrated, leading to the effective Bader charge on the atom. This allows estimating how covalent/ionic/metallic an atom is in the structure. Furthermore, charges that are not localized on but between atoms can be analyzed.

The electronic density of states (DOS) as well as its projection onto the orbitals of the atoms are calculated as implemented in the VASP package.

III. RESULTS

A. Position and definition of the clusters

The quasicrystal approximant used in this study was 1/1-$Al_{78}Cu_{48}Fe_{13}$, with all partial occupancies resulting from structure analysis[24] set to either 1 or 0 (space group $Pm\bar{3}$, 139 atoms per unit cell, $a = 12.329$ Å). After relaxation, the unit cell parameters were 12.270 Å; this is within the generally accepted error of the density functional theory. The total number of atoms is slightly higher (1.9 atoms) in our unit cell, which manifests itself in a slightly higher local symmetry. The already large number of atoms per unit cell does not allow one to approximate partial occupancies and substitutional disorder in supercells.

Figure 1 shows the crystal structure in the cluster description together with its respective ELF. The center cluster at 1/2,1/2,1/2 consists of an Al icosahedron, with a radius of 2.5 Å and edge length of 2.6 Å. The second center cluster shell is an icosidodecahedron of Al with a radius of 4.7 Å and edge length of 2.9 Å, with Fe capping the pentagon faces. They form an icosahedron with radius of 4.7 Å and edge length 4.9 Å. The fourth shell with a radius of 6.5–6.6 Å consists of Cu. All shells of this cluster together represent a Mackay cluster.[25]

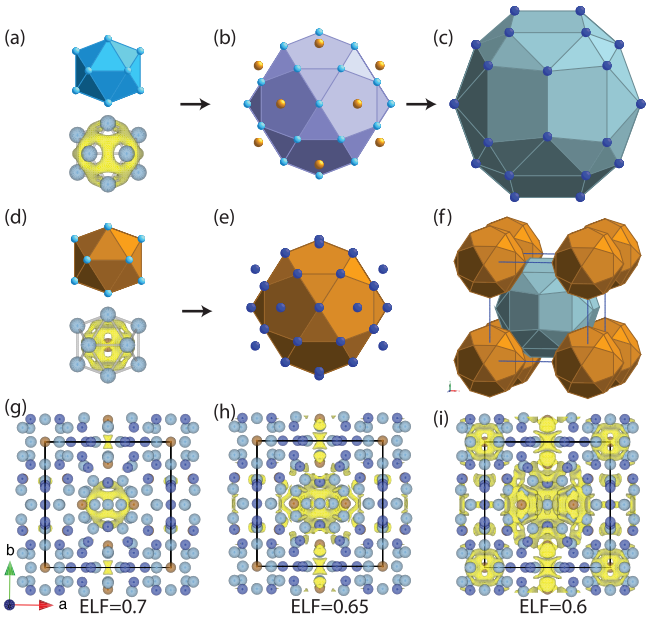

FIG. 1. (Color online) Cluster description of the 1/1-Al-Cu-Fe approximant (Al, light blue; Cu, dark blue; Fe, brown). (a)–(c) Cluster shells centered at the center of the unit cell: (a) Al icosahedron and ELF = 0.7 representation, (b) Al icosidodecahedron with Fe capping the pentagonal faces, and (c) third cluster shell of Cu; (d)–(e) cluster shells centered at the corners of the unit cell: (d) Al icosahedron with Fe in the center and ELF = 0.6 representation, (e) Cu icosidodecahedron with Cu capping the pentagonal faces, and (f) cluster packing; (g)–(i) electron localization function: (g) projection of the unit cell along the c axis at ELF = 0.7, (h) ELF = 0.65, and (i) ELF = 0.6.

The corner cluster is centered at 0,0,0, where an Fe atom is located surrounded by an Al icosahedron with radius 2.6 Å and an edge length of 2.7 Å. The second shell is made of Cu forming an icosidodecahedron with a radius of 4.5 Å and an edge length of 2.7–2.8 Å with additional Cu capping the pentagon faces. They form an icosahedron with a radius of 4.9 Å and edge length of 5.2 Å. The icosidodecahedron that forms the second shell of the corner cluster is connected to the fourth shell of the corner cluster through the Cu, forming the triangular faces of both clusters. The packing of the clusters is depicted in Fig. 1(f).

Figures 1(g)–1(i) illustrate the electron localization function for different isolevels. For the high value of 0.7, the ELF shows a strong localization between the Al atoms of the first shell of the center cluster. Reducing the ELF isolevels to 0.65 shows localized electron density around the second and third shell of the center cluster, between the Fe atoms of the third shell and the Al pentagons of the second shells. A further decrease of the ELF isosurfaces to 0.6 shows localized electron density around the center of the cell and around the Fe atoms at 0,0,0, representing the first shell of the corner cluster. Although increased ELF values are calculated for most of the inner shells of both clusters, those of the center cluster are much higher, indicating a stronger multicenter bonding of Al atoms; see also Fig. 2.

Figure 2 shows a (τ 1 0) ELF cut through the icosahedra of the first cluster shells. The significant differences in the ELF of the two different clusters are clearly visible. The center cluster shows a high ELF (red) between the Al, whereas the corner cluster exhibits a very thin ELF sphere around the central Fe atom.

Figure 3 shows the results of a Bader analysis of the 1/1-Al-Cu-Fe approximant. For Al atoms, the average charge is 1.2 and the Bader volume is 9.4 $Å^3$. Cu shows a charge of

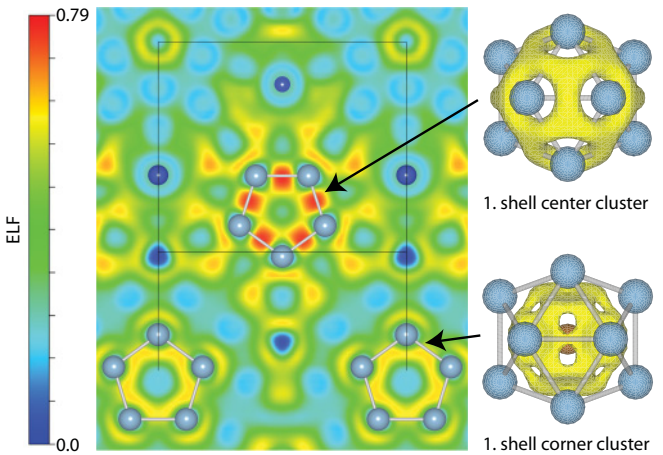

FIG. 2. (Color online) (21 13 0) ELF cut through the icosahedra of the first cluster shells together with the first shells of the center cluster at ELF = 0.7 and the corner cluster at ELF = 0.6. The unit cell is depicted with black lines.

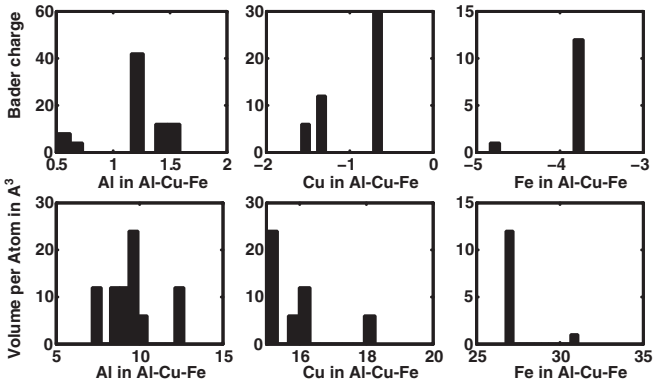

FIG. 3. Bader analysis of the 1/1-Al-Cu-Fe approximant: Bader charges of Al, Cu, and Fe atoms are shown in the upper row; the corresponding Bader volumes are in the lower row.

-0.9 and a volume of 15.8 Å^3. Fe has a charge of -3.8 and a volume of 27.1 Å^3. The histograms show a broad distribution of the Bader charges and volumes of the atoms, caused by different atomic environments. The Al atoms forming the center cluster retain more electrons than the others; this is reflected in the ELF image showing the high concentration around the Al icosahedron. Cu and Fe atoms act as electron acceptors, whereas the Cu atoms around the central cluster attract less electrons, leading to the broad distribution in the Cu Bader charges. This is directly due to the geometrical proximity to the central Al icosahedron and its reluctance to act as an electron donor.

Figure 4 shows the electronic density of states together with its projection onto the atomic orbitals. The general density is strongly influenced by the Cu d states and the Fe d states near the Fermi surface. A narrow pseudogap, with a width of 0.1 eV, is located at 0.1 eV above the Fermi energy that can either be caused by Fermi surface Brillouin zone interactions or by the strong hybridization of transition metal d states with the s and p states of Al. Since our idealized structure model contains slightly more atoms than the experimentally observed 1/1-Al-Cu-Fe approximant, the calculated pseudogap position will be slightly shifted compared to the actual one. The

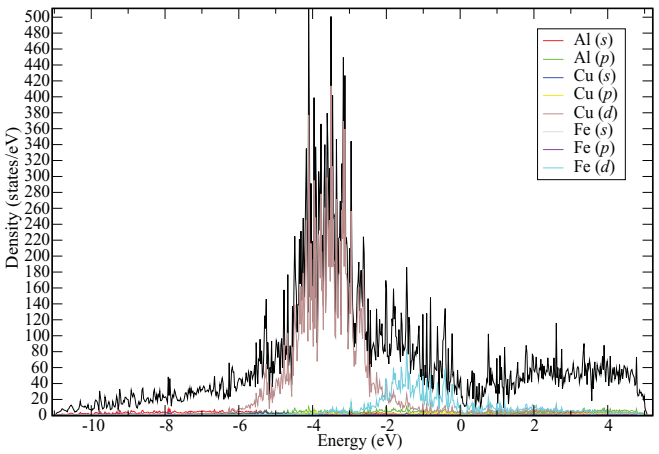

FIG. 4. (Color online) Electronic density of states of the 1/1-Al-Cu-Fe approximant with its projection onto the atomic orbitals. A pseudogap can be identified at ≈ 0.1 eV above the Fermi energy.

influence of a slightly different chemical composition can also be seen comparing our calculations on $Al_{78}Cu_{48}Fe_{13}$ with those by Fujiwara *et al.*[26] on $Al_{80}Cu_{32}Fe_{16}$ as compared to ours. The overall DOS consists of the same spiky curve, as well dominated by the TM d states. The spiky peaks are founded in the superstructure and the repulsive interaction between its components. In their calculation, the pseudogap is shifted away from the Fermi energy to higher energies; this is due to the fact that their structure includes more Fe. In turn, this leads to more occupied d states near and above the Fermi surface.

Additionally one has to say that in the projection scheme used here, the sum over all projections does not add up to the total DOS. VASP does not use localized orbital basis sets, but plane waves as a basis for the electron density. Hence the projected DOS is calculated by weighting the DOS with the projected integrated partial charges, integrated over the volumes of the "atomic spheres."As space cannot be filled by spheres completely, there will always be some discrepancy, and the projected DOS just gives a qualitative picture.

B. Strained cell calculations

The mechanical stability of clusters was studied by trying to create an artificial crack and evaluating the resulting atomic rearrangements. The growth of a crack requires the creation of two new surfaces and hence an increase in the surface energy. Thus the highest probability for a crack would be along the direction of the weakest attractive interactions between atomic layers. For these simulations, the unit cell was doubled along the x direction, creating a $2 \times 1 \times 1$ supercell. The structure was expanded in the same direction, expecting a crack perpendicular to the expansion direction, i.e., the creation of surfaces to lessen the strain within the crystal. The atoms then were relaxed, keeping the unit cell parameters fixed to uphold the strain. This gives the atoms the freedom to find a local energy minimum by local rearrangements. The supercell was first expanded in several steps from 5% to 40% of its original length. An analogous approach was used, for instance, for the study of catalytic properties of $Al_{13}Co_4$ surfaces.[27]

No simulation lead to a formation of a crack just by expanding the structure. Interestingly, the structure was able to incorporate the strain without the formation of new surfaces, i.e., it was uniformly stretched with the expansion of the unit cell. Bader analysis showed just a slight broadening of the histogram for the Bader charges, but no tangible difference in the electron distribution. The broadening, of course, is in direct correlation with the distortion of the cell and the bond lengths; a surface creation, on the other hand, would change the Bader charge histogram due to a different charge distribution on the terminating atoms on the surface.

C. Introduction of cracks/gaps

In order to investigate the effects of cracks, artificial cracks/gaps have been introduced in a $2 \times 1 \times 1$ supercell. The structures were cut and a vacuum gap of 1.5 and 3 Å was added. The gaps have been inserted by intersecting the central cluster ($x = 0.55$) [Fig. 5(a)], between the central cluster and the corner clusters ($x = 0.75$) [Fig. 5(b)], or cutting through the corner clusters ($x = 0.9$) [Fig. 5(c)]. The unit cells

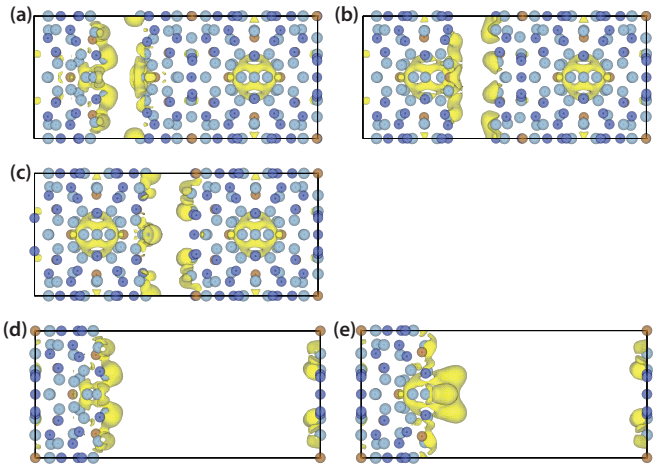

FIG. 5. (Color online) ELF of a $2 \times 1 \times 1$ supercell with a 4-Å gap added at either (a) $x = 0.55$, (b) $x = 0.75$, or (c) $x = 0.9$ for an ELF isolevel of 0.7. ELF of a surface, cut at $x = 0.5$, with flat (d) and artificially restructured (by repositioning of a few Al atoms) cluster termination (e).

were fixed during relaxations and the atoms were given the freedom to move. This resulted in a homogenous distortion of the whole structure, so that the gaps disappeared similar to the strained cell calculations. Interestingly, the structures were able to fuse the gaps, again form their original structure, and incorporate the strain of an additional 3 Å (elongation of ∼12%), at the cost of big forces on the atoms. Consequently, it was not possible to calculate the energies of the different surface terminations because the surfaces disappeared in these structure simulations.

Increasing the gaps to 4 Å, on the other hand, resulted in well-defined flat surfaces on all three cutting sites. The addition of the 4-Å gap, rendering the effective surface distances to ∼5.2 Å, is enough that the energy for fusing the gap is higher than the creation of two surfaces. This is, of course, at 0 K; at higher temperatures the distances would have to be bigger, since the thermal movement of the surface atoms would decrease the effective distance. Figures 5(a)–5(c) show the ELF of the different cuts. At $x = 0.55$, the central cluster is cut in two, and the ELF inside the Al icosahedron has disappeared. Residual electron localization can be found on the terminating surfaces, strongest where the first shell of the center cluster was located. The corresponding cluster shell in the second unit cell remains unchanged. No structural recombination of the atoms forming the cluster takes place. For $x = 0.75$, the cut passes between the central cluster and the corner clusters. Parts of the ELF of the center cluster near the cut moved to the surface, distorting the center cluster slightly. ELF at the surface is localized around the center cluster region.

For $x = 0.9$, the cut passes through the corner cluster. ELF is found at the center region, where the Al-Al bonds have been broken by the cut. Additionally, increased ELF is seen around the Fe, showing the remains of the broken first shell of the corner cluster. Calculations yield that the cracks at $x = 0.55$ and $x = 0.9$ have the same energies, whereas the one at $x = 0.75$ is energetically less favorable (11 meV/atom). This means that the introduction of a gap or crack directly through the first shell of either the corner or the central cluster (breaking of the Al icosahedron) needs the same amount of energy. Surprisingly, the cut at $x = 0.75$ running through the outer shells of the center and corner clusters is energetically least favored. To verify the surface structures of the 4-Å cut, we extended the gaps to 20 Å and the surface termination position remained the same.

D. Artificial surfaces

Artificial structure models have been created to address the issue of flat surfaces cutting the clusters versus puckered surfaces running around them. Using the structure from the cut at $x = 0.55$ with its flat surface, a surface was created where the central cluster was still intact. For this purpose, the flat surface has been restructured by removing four Al atoms from the surface and rebuilding the Al icosahedron (first cluster shell). In this way, a puckered surface is created with an intact first cluster shell jutting out.

Figure 5(d) shows the ELF of the flat surface termination. The ELF within the first shell of the center cluster in the bulk structure has partly disappeared on the surface. The ELF of the restructured cluster surface [Fig. 5(e)] is increased at the surface around the Al icosahedron. The energies of the two structures differ significantly. The flat surface is energetically more favored by 62 meV/atom. This is a big difference, showing that cuts involving complete clusters at the surface will not be stable compared to the flat surfaces.

On the other hand, the integrity of cluster shells could be of importance for the creation of terraced surfaces, as can be found often in experiments. Therefore, models of terraced surfaces have been constructed with different surface terminations. First, a simple step function surface with the flat surface from the $x = 0.55$ cut as termination has been created. Based on this structure model, the surfaces have been restructured, creating intact first shells of the center cluster. Thereby, the Al atoms were taken from the surface layer, analogously to the puckered surface simulations discussed above, in order to be able to compare the energies of the two structures possessing the same number of atoms. For the terraced surface calculations, the Brillouin zone sampling has been lowered to just the Γ point and the self-consistency tolerance has been lowered to 10^{-4} eV per unit cell for

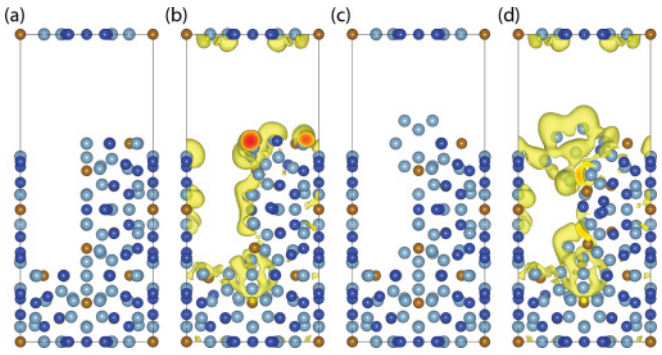

FIG. 6. (Color online) Terraced surfaces: step function (a) and relaxed structure with ELF (b); step function with the first shell cluster termination (c) and relaxed structure with ELF (d). ELF level at 0.7; view along *c* axis.

electronic optimization and 10^{-3} eV per unit cell for atomic relaxation, due to the complexity of the structure.

Figure 6 shows the two different surfaces. For these structures, the cell size has been fixed as well as the atoms with a distance more than 3 Å away from the surface, allowing only surface relaxation. This makes the calculations faster and reinforces the underlying step function surface, which would collapse otherwise. The surface with a flat step function is energetically significantly favored (34 meV/atom) over the puckered one. This shows that also, in the case of terraced surfaces, flat surfaces are preferred over those with intact first shell clusters.

IV. CONCLUSIONS

This study shows that the innermost shells of the fundamental clusters building the 1/1-Al-Cu-Fe approximant of the icosahedral quasicrystal differ in their chemical bonding from the surrounding structure. ELF indicates multicenter bonding between the Al atoms in the icosahedral arrangement, which is also responsible for a narrow pseudogap close to the Fermi energy. However, this does not lead to a particular mechanical stability as proved by our different model calculations. Cuts through the corner and central clusters are energetically equivalent and more favorable than a cut circumventing them. Static equilibrium calculations showed that the surfaces terminated by intact first cluster shells are always less energetically stable than flat surfaces. However, crack propagation in a real experiment does not necessarily create equilibrium surfaces.

ACKNOWLEDGMENT

CSCS Manno is thanked for access to supercomputers.

*steurer@mat.ethz.ch [http://www.crystal.mat.ethz.ch/]

[1] C. L. Henley, M. de Boissieu, and W. Steurer, Philos. Mag. **86**, 1131 (2006).
[2] W. Steurer, Philos. Mag. **86**, 1105 (2006).
[3] M. Conrad, B. Harbrecht, T. Weber, D. Y. Jung, and W. Steurer, Acta Crystallogr. Sect. B **65**, 318 (2009).
[4] M. Duneau and D. Gratias, *Covering Clusters in Icosahedral Quasicrystals*, Vol. 180 (Springer, Berlin/Heidelberg, 2003), pp. 23–62.
[5] P. Steinhardt, H. Jeong, K. Saitoh, M. Tanaka, E. Abe, and A. Tsai, Nature (London) **399**, 84 (1999).
[6] Y. Ishii and T. Fujiwara, Phys. Rev. Lett. **87**, 206408 (2001).
[7] H. Sato, T. Takeuchi, and U. Mizutani, Phys. Rev. B **70**, 024210 (2004).
[8] P. Ebert, M. Feuerbacher, N. Tamura, M. Wollgarten, and K. Urban, Phys. Rev. Lett. **77**, 3827 (1996).
[9] L. Barbier, D. Le Floc'h, Y. Calvayrac, and D. Gratias, Phys. Rev. Lett. **88**, 085506 (2002).
[10] R. D. Diehl, J. Ledieu, N. Ferralis, A. W. Szmodis, and R. McGrath, J. Phys. Condens. Matter **15**, R63 (2003).
[11] F. Rösch, C. Rudhart, J. Roth, H.-R. Trebin, and P. Gumbsch, Phys. Rev. B **72**, 014128 (2005).
[12] L. Ponson, D. Bonamy, and L. Barbier, Phys. Rev. B **74**, 184205 (2006).
[13] L. Barbier, D. Bonamy, and L. Ponson, Phys. Rev. B **78**, 216202 (2008).
[14] F. Roesch and H.-R. Trebin, Z. Kristallogr. **223**, 827 (2008).
[15] G. Kresse and J. Furthmuller, Phys. Rev. B **54**, 11169 (1996).
[16] J. P. Perdew, K. Burke, and M. Ernzerhof, Phys. Rev. Lett. **77**, 3865 (1996).
[17] P. E. Blöchl, Phys. Rev. B **50**, 17953 (1994).
[18] P. E. Blöchl, C. J. Forst, and J. Schimpl, Bull. Mater. Sci. **26**, 33 (2003).
[19] H. J. Monkhorst and J. D. Pack, Phys. Rev. B **13**, 5188 (1976).
[20] A. D. Becke and K. E. Edgecombe, J. Chem. Phys. **92**, 5397 (1990).
[21] B. Silvi and A. Savin, Nature (London) **371**, 683 (1994).
[22] R. Bader, *Atoms in Molecules—A Quantum Theory* (Oxford University Press, New York, 1990).
[23] G. Henkelman, A. Arnaldsson, and H. Jonsson, Comput. Mater. Sci. **36**, 354 (2006).
[24] V. Simonet, F. Hippert, R. A. Brand, Y. Calvayrac, J. Rodriguez-Carvajal, and A. Sadoc, Phys. Rev. B **72**, 024214 (2005).
[25] A. Mackay, Acta Crystallogr. **15**, 916 (1962).
[26] T. Fujiwara, G. Delaissardiere, and S. Yamamoto, Mater. Sci. Eng. A **179**, 118 (1994).
[27] M. Krajci and J. Hafner, Philos. Mag. **91**, 2904 (2011).